Journal of Sol-Gel Science and Technology 6, 83–106 (1996)

Structure Evolution in the PbO-ZrO_2-TiO_2 Sol-Gel System: Part II—Pyrolysis of Acid and Base-Catalyzed Bulk and Thin Film Gels

P.R. COFFMAN, C.K. BARLINGAY, A. GUPTA AND S.K. DEY
Advanced Ceramics Processing Laboratory, Departments of Chemistry, Chemical, Bio, and Materials Engineering, Arizona State University, Tempe, Arizona 85287

Abstract. The pyrolysis behavior of acid and base-catalyzed bulk and thin film $Pb(Zr, Ti)O_3$, or PZT, gels as well as their components have been studied using Thermo-Gravimetric Analysis (TGA), Differential Thermal Analysis (DTA), and Dynamic Mass Spectrometric Analysis (DMSA). The TGA/DTA data reflected the structural differences of the acid and base-catalyzed gels. Gels obtained using an acid catalyst were less cross-linked, denser, and more homogeneous than base-catalyzed gels. Based on the understanding of structure evolution in the silica system, the various events in the TGA/DTA studies of acid-catalyzed PZT gels were attributable to specific mechanisms. The DMSA showed that primarily water, 2-methoxyethanol, acetone, and carbon dioxide were evolved for both acid and base catalyzed PZT gels. The presence of the latter two volatiles was associated with the decomposition of the acetate group via the carbonate route. Acetate and carbonate groups were determined by Fourier Transform Infrared Spectroscopy (FTIR) to be present in the gel structure prior to pyrolysis. Differences in the synthesis of the prehydrolyzed solution were found to affect the amount of residual alkoxy groups, gel structure, pyrolysis behavior, and therefore, the resulting microstructures of sol-gel derived PZT thin films. Finally, some suggestions for improving the processing of sol-gel PZT thin films are given.

Keywords: solution synthesis, gel structures, pyrolytic behavior, processing of PZT powders and films

1. Introduction

In Part I of this series, several spectroscopic and analytical techniques were used to determine the chemical compositions and structures of the prehydrolyzed lead, zirconium, titanium and Pb-(Zr, Ti) alkoxides involved in the sol-gel synthesis of lead zirconate titanate materials [1]. With the eventual goal of understanding the structure-processing-property interrelationships, the next step was to characterize the evolution of the $Pb(Zr, Ti)O_3$ or PZT precursor and its components to the crystalline oxides. A key reason for this study was to initiate an understanding why several research groups, using the same set of precursors, have reported a wide array of microstructures that exhibit a wide range of electrical properties [2–10]. Numerous investigations have studied structural evolution of this system [6–9], but there has not been an integrated approach which follows the evolution of structure from the prehydrolyzed solution to the final ceramic.

In this paper, the sol→gel→ceramic conversion of acid and base-catalyzed bulk and thin film PZT gels, as well as their components, have been studied using Thermo-Gravimetric Analysis (TGA), Differential Thermal Analysis (DTA), Dynamic Mass Spectrometric Analysis (DMSA), Fourier Transform Infrared Spectroscopy (FTIR), X-Ray Diffraction (XRD), and Scanning Electron Microscopy (SEM). It will be demonstrated that differences in the synthetic methods of the prehydrolyzed precursor and hydrolysis conditions (e.g., amount of hydrolysis water, acid/base-catalysis) affect the gel structure, pyrolysis behavior,

phase development, and resulting microstructures of sol-gel derived PZT materials.

2. Experimental

Prehydrolyzed $Pb(Zr_{0.52}Ti_{0.48})O_3$ solutions were synthesized according to the flow scheme in figure 1, using standard Schlenk techniques [11, 12]. This is a modification of a procedure originally reported by Blum and Gurkovich [2]. The titanium and zirconium alkoxides were refluxed separately, deliberately avoiding formation of the bimetallic alkoxide. Consequently, the reactivity of the titanium and zirconium alkoxides in the complexation reaction of the lead precursor was expected to promote the replacement of the acetate ligands with alkoxide ligands [1]. This strategy should minimize the amount of acetate groups, which do not undergo hydrolysis, and thereby give a cleaner pyrolysis. In order to interpret the results from the PZT system, the $PbTiO_3$ (PT) and TiO_2 (T) systems were investigated when necessary.

Titanium methoxyethoxide, $Ti(OCH_2CH_2OCH_3)_4$, was synthesized by refluxing titanium isopropoxide

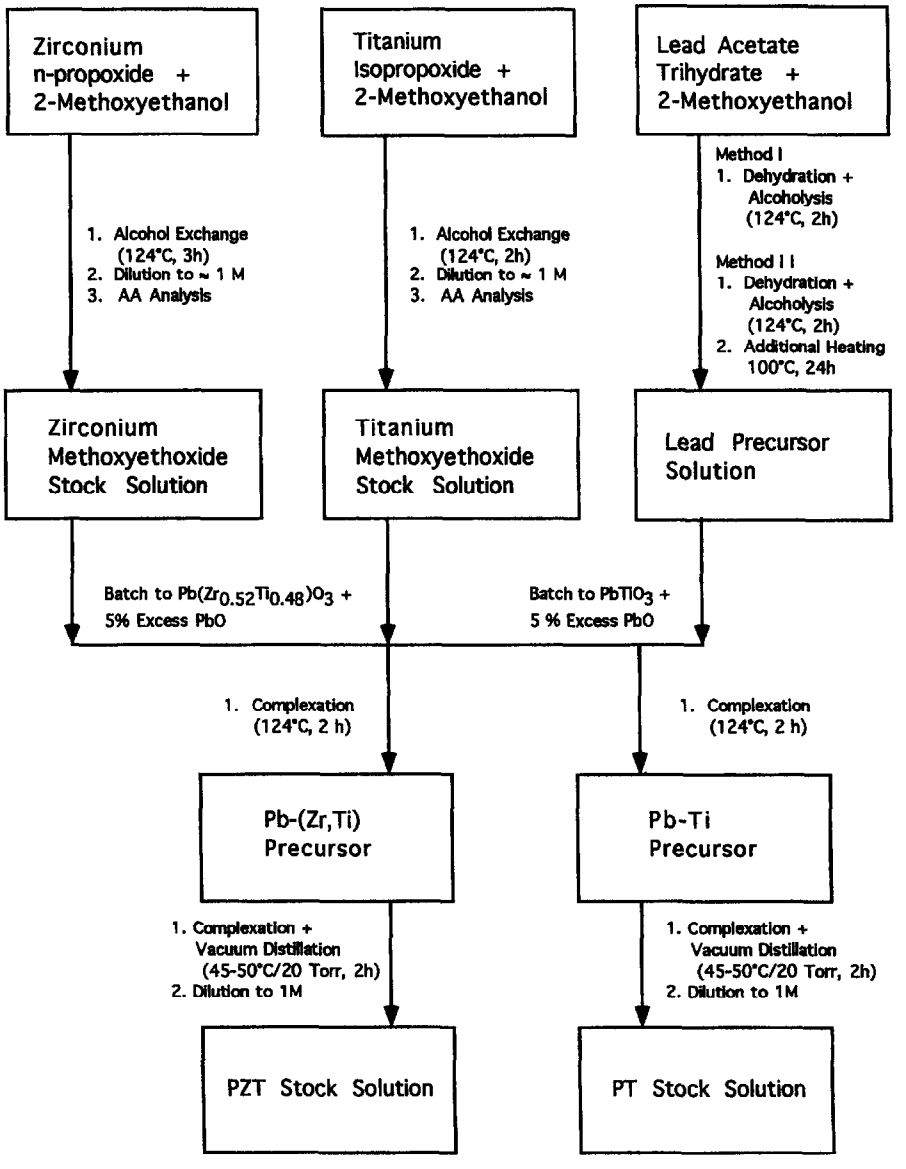

Figure 1. Flow diagram for the synthesis of Ti, Zr, Pb-Ti and Pb-(Zr, Ti) alkoxides.

(Alfa, 99.99%) in 2-methoxyethanol, ROH (Aldrich HPLC grade), at 124.5°C for 2.0 hrs, while removing isopropanol by distillation. The titanium alkoxide was then diluted to give a 1.06 M stock solution which was confirmed by atomic absorption (AA) spectroscopy. Zirconium methoxyethoxide, $Zr(OCH_2CH_2OCH_3)_4$, was synthesized by refluxing zirconium *n*-propoxide (Alfa, 99.99%, 70 wt%) solution in *n*-propanol) in ROH at 124.5°C for 3.0 hrs, while removing *n*-propanol by distillation. The zirconium alkoxide was then diluted with ROH to give a 0.88 M stock solution as determined by AA.

In the synthesis of lead-based prehydrolyzed precursors, two methods (I and II) were utilized. In the first method, lead acetate trihydrate, $Pb(OOCCH_3)_2 \cdot 3H_2O$, or $Pb(Ac)_2 \cdot 3H_2O$ (Alfa, 99.999%), was refluxed in ROH at 124.5°C for 2.0 hrs to remove the water of hydration by distillation. PZT prehydrolyzed solutions were synthesized by mixing this lead precursor with the Zr and Ti alkoxide solutions followed by refluxing and distilling for 2.0 hrs at atmospheric pressure. The Pb-(Zr, Ti) alkoxide was then vacuum distilled at 45–50°C at 20 Torr for 2.0 hrs, then cooled and diluted to a concentration of 1.0 M. Note that this procedure will now be referred as method I. Prehydrolyzed PZT solutions containing a 5% excess lead over the stoichiometric composition were synthesized by this method. A stoichiometric lead titanate prehydrolyzed solution was also made by this route. Most of the studies in this paper were performed on gels made by method I. The second method, hereafter referred to as method II, was the synthetic scheme reported in part I of this series. In method II, following the initial refluxing (distillation) of $Pb(Ac)_2 \cdot 3H_2O$, the lead precursor solution was further heated at 100°C for 24 hours before mixing and refluxing with the Zr and Ti alkoxides. Part of the prehydrolyzed PZT precursor solutions made by methods I and II were evaporated to dryness at 60°C/0.07 Torr to their respective oils.

To fabricate gels, the precursor solutions were hydrolyzed by adding 1.5 to 3.0 moles H_2O per mole of Pb-(Zr, Ti) alkoxide and an acid (HNO_3) or base (NH_4OH) catalyst to give a 0.075 M concentration in the sol (i.e., hydrolyzed solution). The resulting concentration of the sols was 0.5 M with respect to stoichiometric PZT. Sols of PZT, PT, and T were aged for 24 hours, and gels were obtained by drying these sols in an oven at 120°C for 24 hrs. Some acid and base catalyzed PZT gels were freeze-dried to remove residual solvent which yielded very fine, golden colored powders. This was done to preserve the room temperature gel structure. Table 1 designates all the gels prepared in this study along with composition, synthetic method, and hydrolysis conditions. The nature of the prehydrolyzed precursors and their pyrolysis behavior were determined using several analytical techniques. The differences between the PZT prehydrolyzed solutions obtained by methods I and II and the resulting ceramics will be demonstrated.

Table 1. Designation of gels by composition, synthetic method and hydrolysis conditions.

Composition	Synthetic method	Moles water per mole of alkoxide	Catalyst	Designation
PZT, PT, T	I	1.5	Acid	A1
PZT, PT	I	1.5	Base	B1
PZT	I	2.0	Acid	A2
PZT	I	3.0	Acid	A3
PZT	II	1.5	Acid	A4
PZT	II	1.5	Base	B2

Thermo-Gravimetric Analysis and Differential Thermal Analysis (TGA/DTA) was provided by a Setaram TG 92. Platinum crucibles which had been pre-reacted with PZT powder were used to contain the gels. This step was necessary due to the slight reaction between PZT and platinum. A scan speed of 5°C per minute on the heating ramp was used to maximize both resolution and sensitivity, utilizing 50 mg samples. A background run was performed using the pyrolyzed sample under identical conditions after the initial raw run, and was then subtracted from the raw data.

A Varian MAT 312 mass spectrometer was utilized for the dynamic mass spectrometry analyses. Samples were heated to 470°C in high vacuum (typically 10^{-6} Torr) using a solids probe. Mass spectra of the decomposition products were then recorded as a function of temperature. The background fragmentation pattern of air was obtained prior to collecting the sample spectrum, and the actual spectrum was then obtained from the difference. The mass spectra were then compared to standard spectra of the pure compounds [13].

Infrared spectra were obtained from an FTIR spectrophotometer (Mattson, Galaxy 2020). Oils were studied by FTIR as films on KBr windows. Solids were analyzed by dispersing in KBr and then pressing into pellets. The vacuum (10^{-5} Torr) decomposition products of an acid-catalyzed freeze-dried (−85°C/0.01 Torr) gel were analyzed by gas phase spectroscopy with a 10 cm pathlength gas cell.

Films were formed by spin-casting the 0.5 M sols, which were aged 24 hours, as described above. These solutions were deposited on Pt/Ti/SiO_2/Si (100) wafers at 2000 rpm. The required final film thickness was achieved by multiple deposition steps, with heating at 350–400°C between layers.

Heat treating films was accomplished by both conventional firing (15°C/min) and rapid thermal annealing, RTA, which had a heating rate of 250°C/sec. An RTA furnace, AG Associates Heatpulse 610, was utilized for these experiments.

X-ray diffraction patterns were obtained on a Rigaku D-Max IIB diffractometer. A Hitachi 5000-S SEM was used to determine the grain size and morphology of the PZT thin films prepared by methods I and II.

3. Results and Discussion

3.1. TGA/DTA and DMSA Observations of Pyrolysis Behavior in Inert Atmospheres and Vacuum

In order to correlate thermal events and mass losses with volatile decomposition products, DMSA analyses were performed in coordination with TGA/DTA experiments. The summary of all TGA/DTA and DMSA experiments is listed in Table 2. It includes the type of

Table 2. Summary of all TGA/DTA and DMSA experiments.

Figure#	Sample	Method	Atm.	%wt loss	Temperature°C /Thermal Event	Volatile Products	Process
2a	A1 PZT	I	He	24.9	20–220 endo	H_2O, ROH	Desorption
					220–290 exo	ROH	Condensation
					328 exo		Pb melting
					290–380 exo	Acetone, CO_2, ROH	
					360–600 exo	CO_2	
4a	A1 PT	I	He	23.5	same	same	
2b	B1 PZT	I		25.5	20–100 endo	H_2O, ROH	
					220–290 endo	ROH	
					328 exo		Pb melting
					360–600 endo	Acetone, CO_2, ROH	
						CO_2	
4b	B1 PT	I	He	22.5	same		
5	A1 T		He		20–120 endo		
					120–160 exo	Volatiles	
					220–240 endo	Not studied	
					240–320 exo		
					430–500 endo		
6a	PbAc		He	37.6	20–180 endo	H_2O	
					80 endo	Pb phase change	
					180–220 endo	Acetone	
					220–270 endo	Acetone, CO_2	
					328 exo		Pb melting
					320–360 endo	CO_2, Acetone	
					360–700 endo	CO_2	
6b	$PbCO_3$		He	17.6	230–270 endo		
					300–340 endo	CO_2	
					590–650 endo		
8b	A2 PZT	I	He	24.2			
8c	A3 PZT	I	He	21.7			
12a	A1 PZT	I	O_2	19.2			
12b	B1 PZT	II	O_2	18.3			
14a	A4 PZT	II	He	15.2			
15	A4 PZT	II	O_2	12.6			

atmosphere, thermal events, percent weight loss, volatile products identified, and process involved in each thermal event.

3.1.1. Acid and Base-Catalyzed PZT Gels. The TGA/DTA results for A1 PZT in a helium atmosphere are shown in figure 2a, while the DMSA results are presented in figure 3. The TGA/DTA of A1 PZT exhibited a broad endothermic weight loss between 20–220°C. The main products were ROH and H_2O, as determined by DMSA. In this temperature regime, water loss decreased while methoxyethanol loss increased. This indicated that mainly adsorbed water and solvent were being lost. A large exothermic peak with a maximum at 250°C occurred over a temperature range of 220–290°C. This exotherm corresponded to a rapid weight loss in TGA. The main product was ROH, with some evolution of acetone and CO_2. Additionally, two exothermic peaks were seen from 290–380°C, with the first being a broad event taking place over this entire range and reaching a maximum at 340°C. In this region, the main decomposition products were found to be acetone, CO_2, and ROH. The second peak, centered at 328°C, was an event occurring over only a few degrees. From 380–600°C, a broad exotherm was observed. In the region of 380–455°C, only acetone and CO_2 were observed, and after 455°C, only pure CO_2 was seen. A similar decomposition behavior for A1 PZT was observed under a reducing condition using forming gas (8% H_2 and 92% N_2).

The TGA/DTA of B1 PZT (figure 2b) exhibited a defined endothermic response over the temperature range of 20–100°C, and corresponded to a higher rate of weight loss than in A1. In contrast to A1, B1 exhibited a small, but broad endotherm between 220–290°C. A similar thermal feature that was present in A1 PZT was also present in B1 between 290–380°C, except that it was not exothermic. Also, a sharp exotherm was present at 328°C. From 380–600°C, a broad exotherm was observed. A similar decomposition behavior for B1 PZT was observed under a reducing condition using forming gas.

3.1.2. PT and T Gels. In order to gain better understanding of the pyrolysis behavior of PZT gels, A1 and B1 PT were studied. The TGA/DTA of PT gels in helium were very similar to the corresponding PZT gels. An exothermic event centered at 250°C was also noted in A1 PT (figure 4a), but not in B1 PT

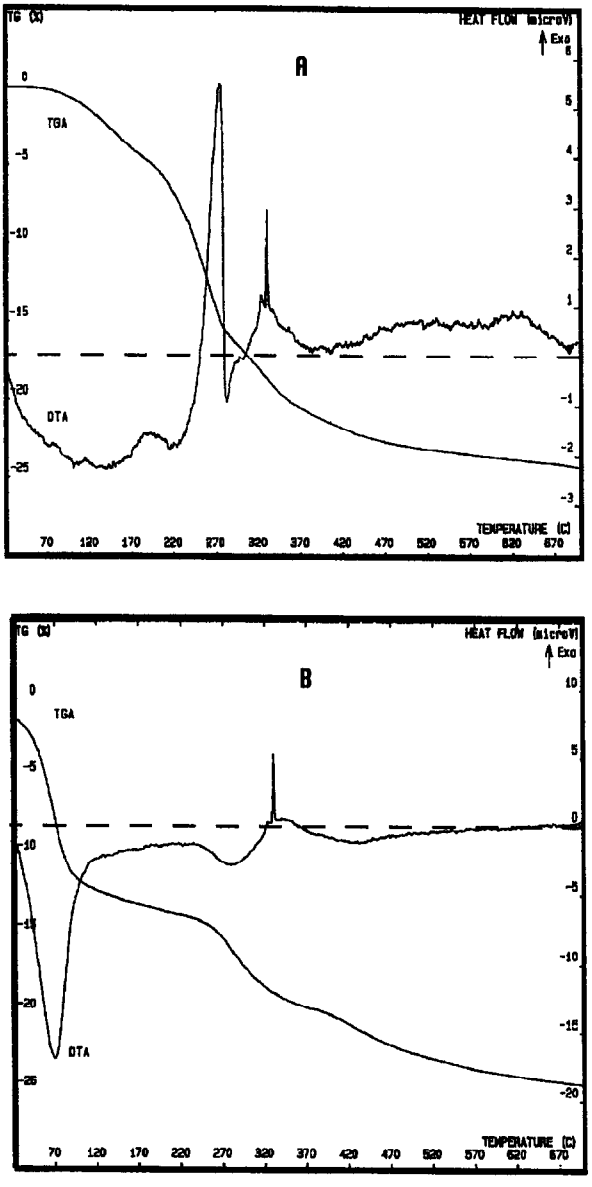

Figure 2. TGA/DTA curves for (a) A1 and (b) B1 PZT gels in helium.

(figure 4b). The sharp exothermic peak observed at 328°C was also observed in both A1 and B1 PT. The decomposition products of A1 and B1 PT were identical to those observed with A1 and B1 PZT. To correlate the exothermic peaks to individual metal precursors, the components of the PT system were further studied by analyzing T gels and PbO precursors. A1 T gels were pyrolyzed in the TGA/DTA (figure 5), and four exotherms were found compared to three observed for PZT. These peaks were found at 150, 230, 300, and

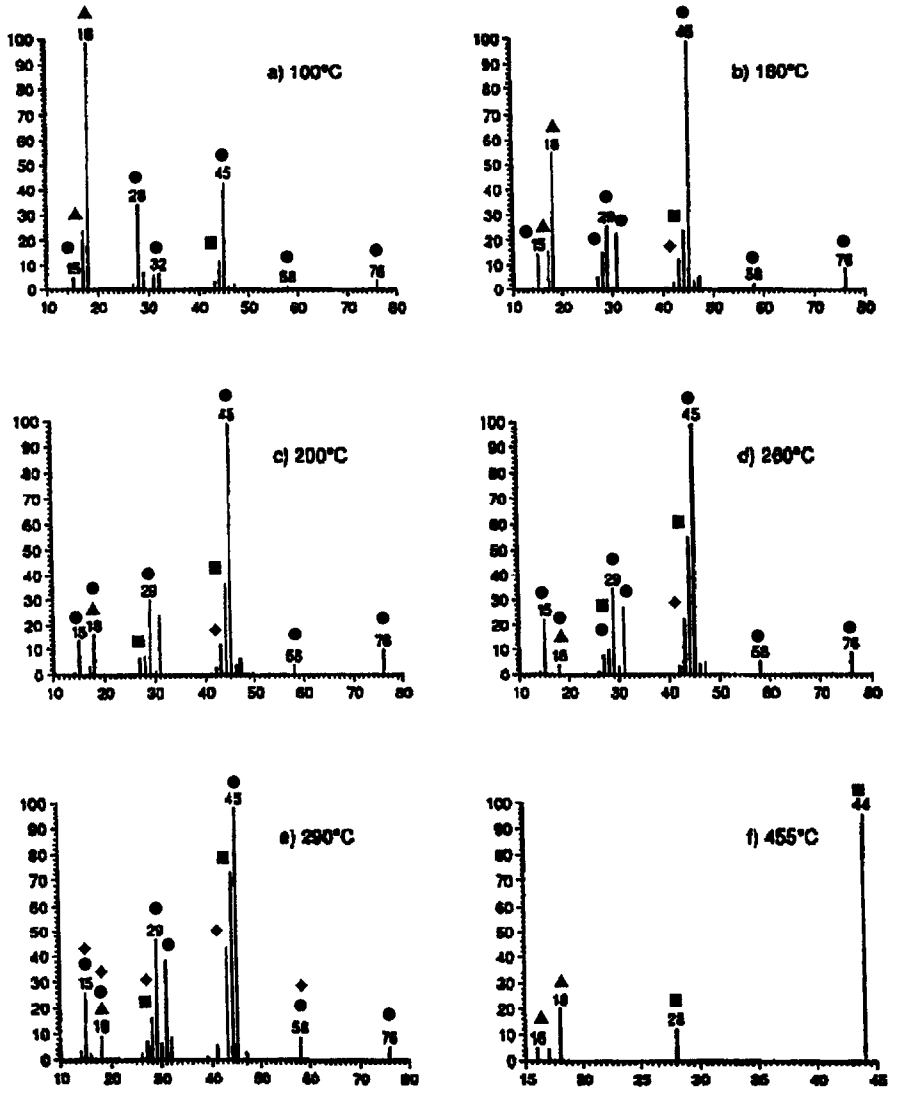

Figure 3. DMSA results for PZT gels (▲ = water, ● = 2-methoxyethanol, cetone, ■ = carbon dioxide).

470°C, with the largest one being at 300°C. Unlike A1 PZT and PT, a sharp exothermic peak at 328°C was not observed in A1 T. This peak therefore, may be associated with the lead precursor. To ascertain this, lead acetate trihydrate and lead carbonate (the rational for its use will be evident later) were decomposed in helium.

3.1.3. Lead Compounds. The TGA/DTA curves for lead acetate trihydrate (figure 6a) showed four endothermic peaks at 180, 250, 280, and 340°C. Additionally, a sharp inflection was observed at 328°C overlaid on the large endothermic peak at 340°C. The spectra collected for the in-situ calcination products of lead acetate trihydrate at different temperatures are shown in figure 7. Primarily, the evolution of water at about 65°C, followed by acetone at 200–330°C was observed. The secondary species was CO_2 in the 200–330°C regime. After 330°C, CO_2 became the dominant species and acetone decreased, and after 420°C, pure CO_2 evolved. The dynamic fragmentation pattern for acid-catalyzed PZT gels was quite similar to that for pure lead acetate trihydrate, as seen in figure 7. The acetate ligands can undergo thermal decomposition with the liberation of acetone and carbon dioxide. Lead carbonate is an intermediate in the decomposition

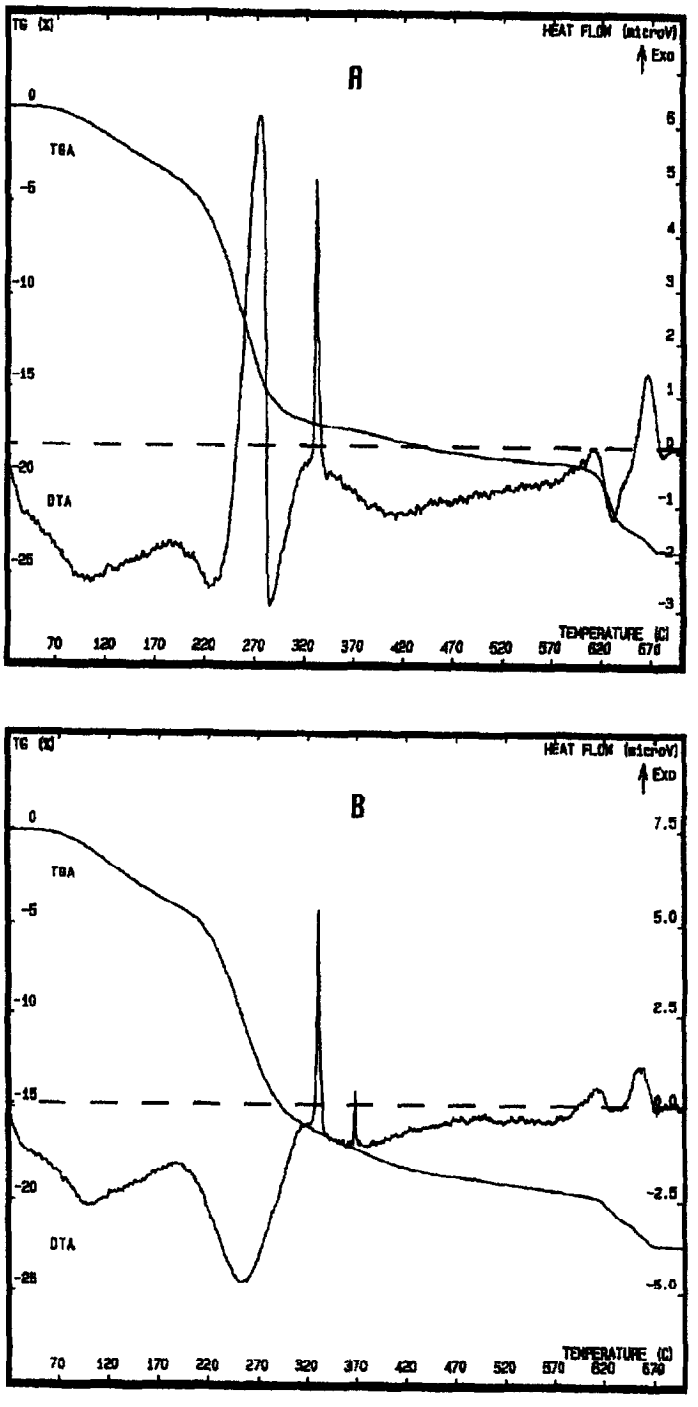

Figure 4. TGA/DTA results for (a) A1 and (b) B1 PT gels in helium.

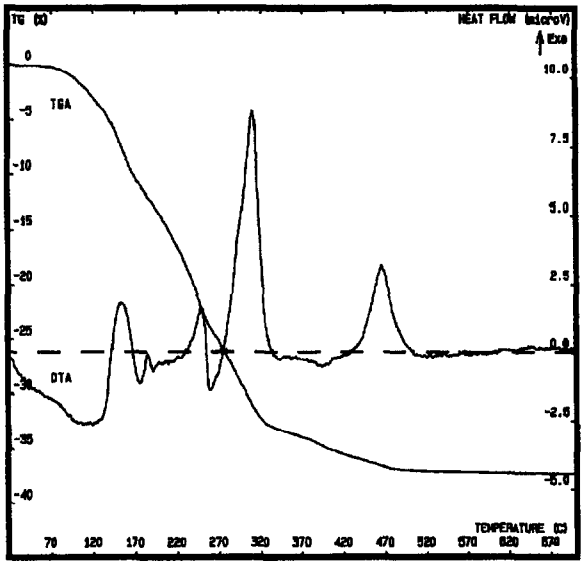

Figure 5. TGA/DTA curves for A1 T gels in helium.

process as shown below.

$$Pb(OOCCH_3)_2 \longrightarrow PbCO_3 + CH_3COCH_3 \quad (1)$$

$$PbCO_3 \longrightarrow PbO + CO_2 \quad (2)$$

Both reactions are endothermic, with values of $\Delta H°$ computed to be 47.7 and 88.6 KJ/mole for reactions 1 and 2, respectively. Other decomposition pathways are also possible, as shown by the higher mass peaks in the mass spectrum taken at 330°C (figure 7d).

The XRD patterns of PZT, PT and the lead acetate trihydrate pyrolyzed at 700°C in the TGA/DTA analyzer under a helium atmosphere indicated the presence of metallic lead. The formation of metallic lead in the present study is supported by a couple of key observations. First, gels pyrolyzed in helium and oxygen ambients were black (due to carbonaceous residues and metallic lead) and yellow (due to oxide), respectively. Second, the decomposition of lead carbonate in helium (figure 6b) gave a yellow solid. The DTA of lead carbonate showed two large endothermic peaks at 250 and 300°C, as well as a broad endothermic feature from 590–650°C, but no exothermic peak at 328°C. The absence of metallic lead in this case can be explained since the thermodynamically favored decomposition products are PbO and CO_2 only. Thus, the origin of the elemental lead during the pyrolysis under He stems from the reduction of Pb—O species in $Pb(Ac)_2 \cdot 3H_2O$, PT, and PZT. The source of the reducing conditions to form metallic lead is carbonaceous residues created from the decomposition of organic ligands in helium. The origin of this reducing environment was due to the creation of carbon and carbon monoxide which can dreduce the oxides of lead. This reduction occurred over a wide temperature range, therefore it was not observed during the raw run. As a result, Pb melted (328°C) endothermically during the background run, but exhibited an exotherm when subtracted from the raw data.

It is of interest to note the differences in the normalized peak height (μV/mg) of the lead melting peak. In the case of acid-catalyzed PZT gels, the values were approximately 0.05 to 0.06. In the case of base-catalyzed PZT gels, these values ranged from 0.10 to 0.13. Thus, there was significantly more metallic lead produced in base-catalyzed gels than acid-catalyzed gels in the carbon-rich reducing environment. This is due to the fact that both base-catalyzed PZT and PT gels were found to have an inhomogeneous distribution of Pb and Zr/Ti on the atomic level (as will discussed in the next section). There is clear evidence of Pb—O—M (M = Zr and/or Ti) bonds in the prehydrolyzed solution based upon ^{207}Pb NMR [1]. In dried acid catalyzed gels, the persistence of such heterometallic bonds results in nanocrystalline regions (observed as perovskite PZT by TEM [15]). However, in uncatalyzed and base catalyzed gels, MAS NMR and/or EXAFS studies are needed to determine the extent of the Pb—O—M bonding upon gelation. In basic gel networks, there are regions rich in Pb—O—Pb bonds, facilitating lead reduction. In essence, the Pb—O species being reduced arise from both a) deliberately added excess PbO and b) PbO rich regions in the PZT gel. The latter is caused by inhomogeneity induced during hydrolysis and condensation reactions.

With the exception of the aforementioned exothermic peak at 328°C, the differences in the DTA patterns between acid and base catalyzed gels must stem from another source. The exotherms in A1 PZT and PT (at 220–290°C, 290–380°C, 380–600°C) cannot be associated with lead-oxygen species since both lead acetate trihydrate and lead carbonate exhibited endothermic decomposition patterns. Therefore, the exothermic events seen in A1 PZT, PT, and T are most likely due to the effect of gel structures as will be described in the next section.

It is of practical interest to note that a high decomposition temperature (650°C) of lead carbonate was observed. Any existing carbonate groups below

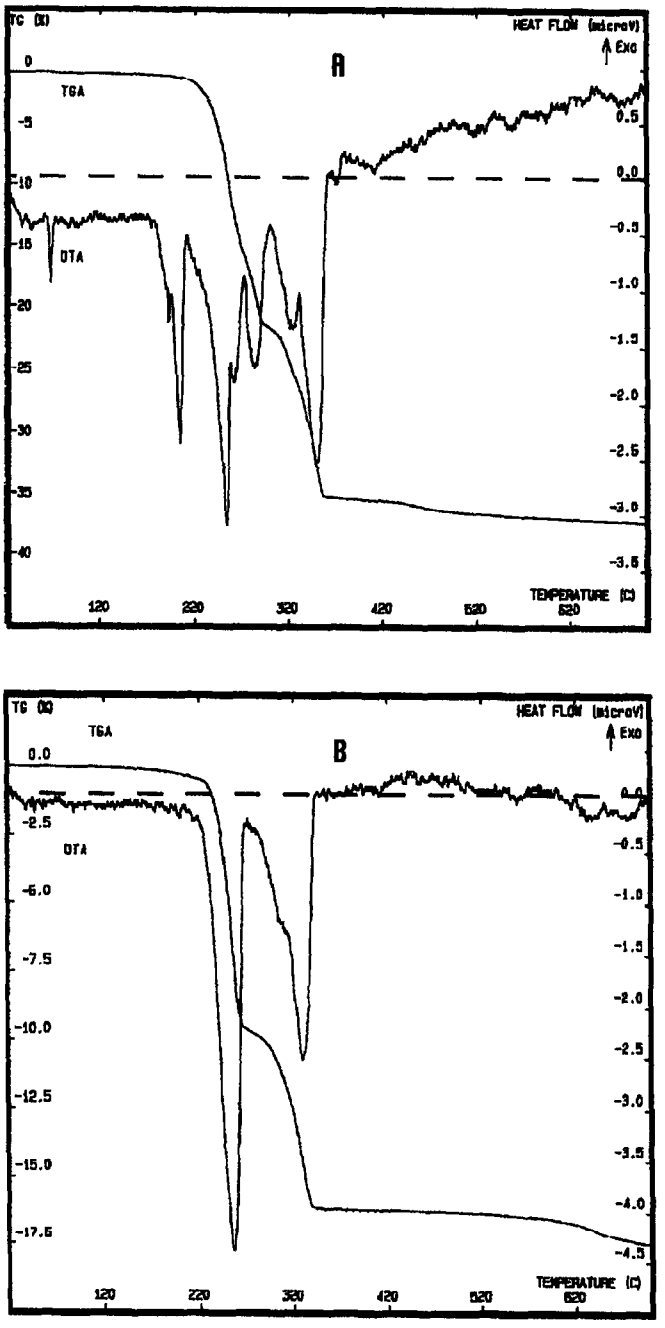

Figure 6. TGA/DTA results the decomposition of (a) lead acetate trihydrate in helium and (b) lead carbonate in helium.

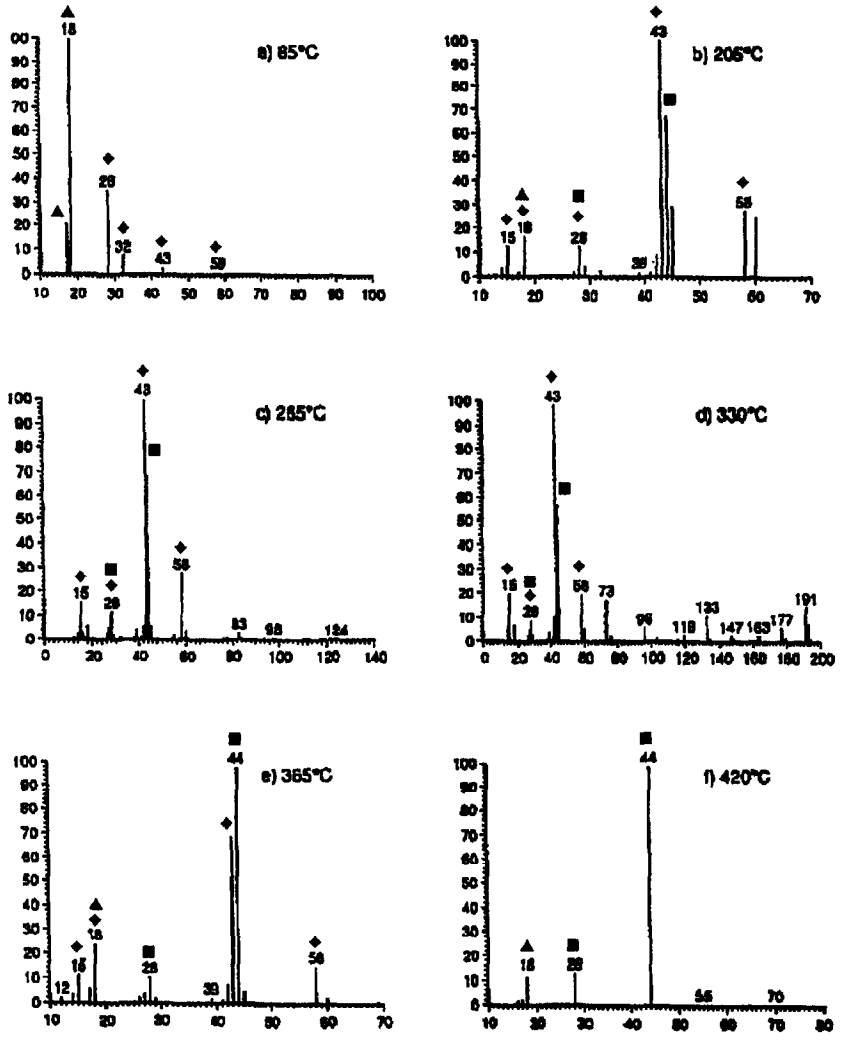

Figure 7. DMSA results for lead acetate trihydrate (▲ = water, ● = 2-methoxyethanol, ♦ = acetone, ■ = carbon dioxide).

the surface of a gel or in the gel structure will lead to a higher decomposition temperature, which is undesirable.

3.1.4. PZT Gel Structures Obtained from Acid and Base Catalysis. The differences in physical characteristics of acid and base-catalyzed PT gels have been reported to be analogous to silica gels [15]. PT gels formed from acid-catalyzed solutions were clear and rubbery, whereas base-catalyzed gels were cloudy and phase separated with the solvent due to their cross-linked nature. Direct TEM observations determined that the former were fibrous in character and physically homogeneous, whereas the latter had a coarse texture. Acid-catalyzed gels also had a homogeneous distribution of Pb and Ti. This indicated that the less cross-linked, homogeneous acid-catalyzed gels were capable of polymeric rearrangement during drying, yielding low energy structures containing microcrystalline regions. In contrast, highly cross-linked base-catalyzed gels had an inhomogeneous distribution of Pb and Ti. This would necessitate a reconstructive transformation before crystallization can occur. Similar behavior was documented for acid and base catalyzed PZT gels. In-situ HREM observations on structure evolution in the PZT system [16] indicated that acid-catalyzed gels decomposed and crystallized at lower temperatures than base-catalyzed gels. At about 300–400°C, the acid-catalyzed gels attained a very low energy amorphous structure to the extent of

being nanocrystalline. In contrast, metastable base-catalyzed gels required significantly more energy to undergo a sluggish reconstructive transformation to the crystalline state, resulting in higher crystallization temperatures. These reports on the characteristics of acid and base-catalyzed gels coupled with the proposed pyrolysis mechanisms for the silica system, may be used to interpret the current data (TGA/DTA/DMSA).

Based on the shrinkage and weight loss data for the silica system [17], three distinct regions during pyrolysis were identified: 1) Region I (up to 150°C): weight loss with little or no shrinkage; desorption of solvent and capillary contraction. 2) Region II (150–520°C): shrinkage proportional to weight loss; shrinkage due to both polymeric particle rearrangement (increased packing efficiency) and skeletal densification. Skeletal densification occurred by condensation polymerization and structural relaxation. Note that both particle rearrangement and structural relaxation cannot contribute to weight loss. 3) Region III (above 520°C): shrinkage without weight loss; characterized by viscous sintering. It was apparent that these regions do not have well defined boundaries and significant overlap was observed. Interestingly, current pyrolysis data for A1 PZT (mostly exothermic) and B1 PZT (mostly endothermic) gels indicate the presence of species in different chemical environments (i.e., different structures) that could lead to different pyrolysis mechanisms (Table 2, column 6).

For acid-catalyzed PZT gels, particle rearrangement and/or skeletal densification are expected to occur throughout the temperature range of 220–600°C, but the dominant mechanism may vary in a particular temperature range. The weight loss associated with the exothermic peak at 220–290°C was higher than the peak at 290–380°C. Additionally, DMSA results indicated that from 220–290°C, the major pyrolysis constituents were ROH, while from 290–380°C, acetone and CO_2 were the major products. Therefore, the dominant mechanism for the exothermic decomposition from 220–290°C is condensation polymerization between alkoxy and hydoxy groups, while from 290–380°C, the major mechanism is the decomposition of acetate groups along with some condensation polymerization. The broad exothermic peak between 380–600°C can be attributed to either structural relaxation or particle rearrangement since very little weight loss was associated with it. The latter mechanism probably dominates since dried acid-catalyzed PZT gels exhibited the tetragonal modification in TEM studies at low temperatures (300–400°C) [18]. In essence, a high degree of structural relaxation must have occurred at a relatively lower temperature (below 380°C). To reinforce the origin of the exothermic behavior in acid-catalyzed gels and to gain further insight into the structural differences of acid and base-catalyzed gels, the amounts of hydrolysis water were varied.

Increasing the amount of hydrolysis water should help hydrolyze more alkoxide groups, thus, giving rise to increased cross-linking. Consequently, the released exothermic energy associated with particle rearrangement and skeletal densification is expected to decrease, and indeed, this was observed. As the amount of hydrolysis water is increased from 1.5 moles (A1 gels) to 3.0 moles (A3), the broad exotherm between 380–600°C decreased (figure 8) along with the weight loss (from 24.9 to 21.7%). This confirms that the exothermic peak between 380–600°C is due to modification of a less cross-linked structure. In this work, the high water acid-catalyzed gels begins to approach the behavior of base-catalyzed gels containing a lower amount of water with respect to weight loss and structure (as observed by DTA events). To distinctly separate the individual mechanisms would require shrinkage, and pore characteristics data. In the complex Pb-based perovskite system, however, these mechanisms are compressed within a very narrow temperature range, since crystallization is also complete by 635°C. Therefore, a distinct separation of the individual mechanisms could be difficult.

3.2. *FTIR Studies*

The amounts of alkoxy, hydroxy, acetate, carbonate and oxide groups can vary with the conditions of gel formation (e.g., solution synthesis, hydrolysis, catalysis, drying conditions, etc.). Thus, FTIR was used to compare the amounts of these groups as a function of the processing conditions.

Infrared spectra (absorbance, 3.8 m.g.) of the Pb-(Zr, Ti) prehydrolyzed precursor synthesized by methods I and II are displayed in figure 9(a, b), respectively. At high frequency (centered at around 3375 cm^{-1}), the broad band of the O—H stretch (1) was present. These could be due to the alcoholic $CH_3OC_2H_4O$—H stretch, since a band was observed at 3398 cm^{-1} in the free alcohol. The source of the alcohol was not due to residual solvent from the Pb-(Zr, Ti) alkoxide, but most likely stems from the formation of a solvate in

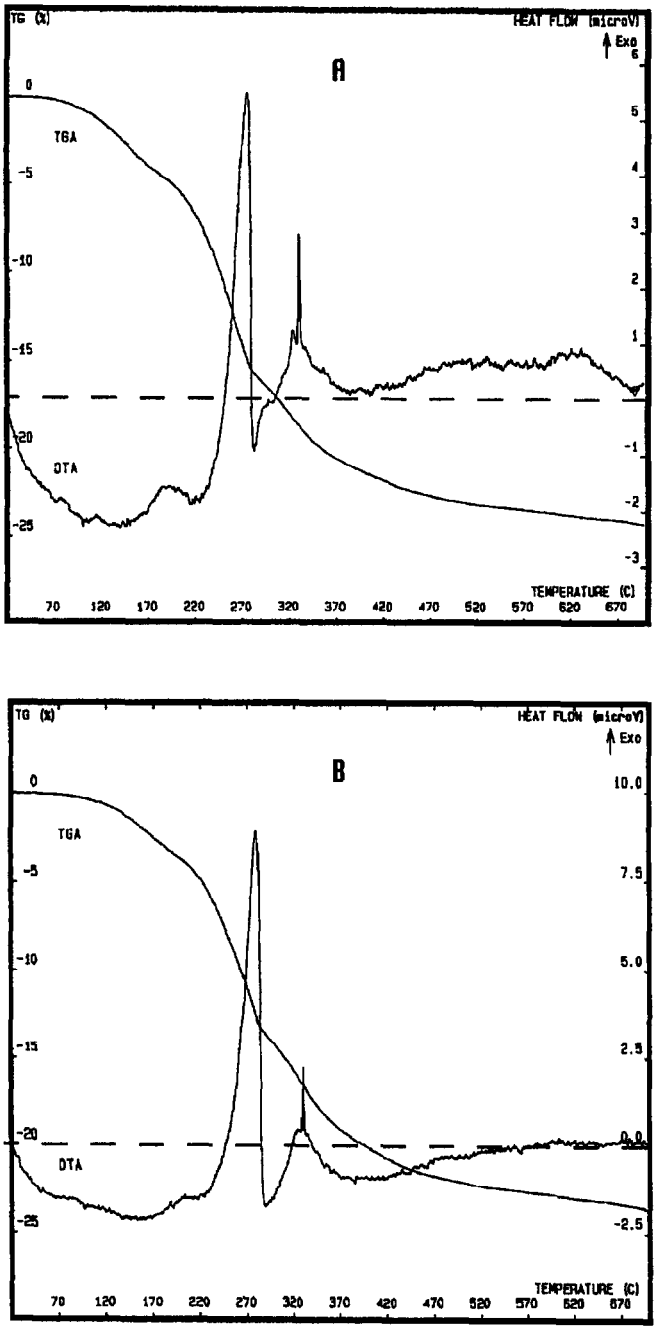

Figure 8. TGA/DTA results for acid-catalyzed PZT gels with different amounts of hydrolysis water: (a) A1 (1.5 moles water/mole alkoxide) (b) A2 (2.0) (c) A3 (3.0).

(Continued.)

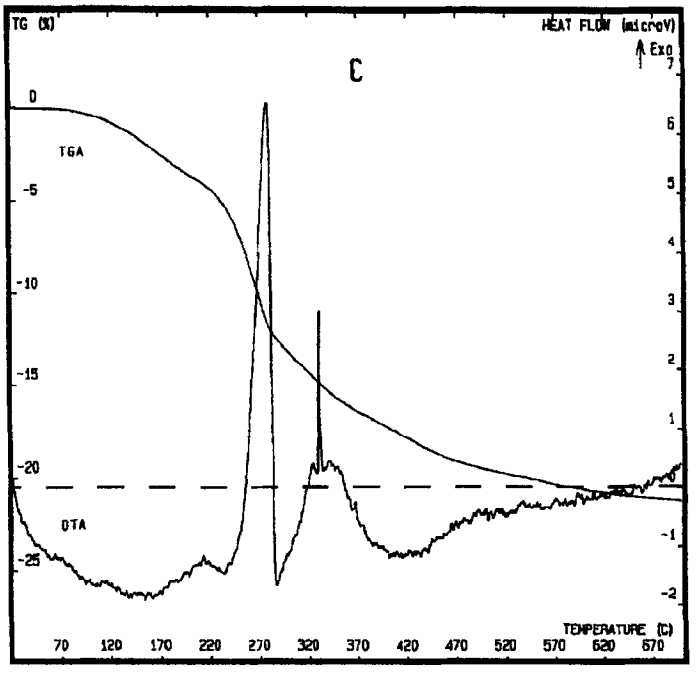

Figure 8. (Continued)

the oil. The C—H stretching bands (2) were observed at 2830–2976 cm^{-1}. The assymetric (3) and symmetric stretches (4) of the acetate carboxylate group were at 1572 and 1451 cm^{-1}, respectively. The difference in frequency between the two was 121 cm^{-1}, which is indicative of a bridging configuration for the acetate group [29]. Between 1020–1240 cm^{-1}, C—O stretching bands (5) were observed. At 908 cm^{-1}, a C—H bending mode (6) was observed. A sharp peak at 837 cm^{-1} due to the carbonate group is seen (7). And at 484 and 575 cm^{-1}, the Ti—O and Zr–O stretches (8) were observed, respectively. Figure 9c shows the difference of 9b subtracted from 9a. The difference in these two spectra was the bands due to the —OR group, which were more intense in the method I than in the method II precursor. This was seen by the bands due to C—H (2830–2976 cm^{-1}) and C—O (1020–1240 cm^{-1}). Therefore, there is a higher amount of residual methoxyethoxide ligands in the prehydrolyzed precursor prepared by method I compared to method II. The smaller amount of —OR groups in the prehydrolyzed precursor synthesized by method II is due to the fact that the extra 24 hours of heating at 100°C causes more condensation to occur, more Pb—O—Pb bonds to form, and more —OR groups to be eliminated in the form of ROH. Thus gels prepared via method II have a lower weight loss upon pyrolysis (15.2% vs. 24.9% for A1 PZT).

Figure 10(a, b, c) shows the Infrared spectra of lead carbonate, lead acetate trihydrate, and a freeze-dried A1 PZT gel, respectively. The spectrum of the freeze-dried A1 PZT gel showed a bands due to the O—H stretch (1). Peaks for residual alkoxides were seen between 2800–3000 cm^{-1} which was due to the C—H stretch (2). The strongest peaks identified were those corresponding to the acetate group at 1559 cm^{-1} and 1384 cm^{-1}, corresponding to the asymmetric (3) and symmetric (4) stretching vibrations of the acetate carboxylate group. The difference in frequency between the two was 175 cm^{-1}, which is indicative of a bridging configuration for the acetate group [18]. Between 1000–1250 cm^{-1}, C—O stretching bands (5) were observed. At 750 to 1000 cm^{-1}, the C—H bending modes (6) were observed. A peak at 835 cm^{-1} was observed, which corresponds to the CO_3 group (7), which is observed at 839 cm^{-1} in $PbCO_3$ (figure 10b). And at 500 cm^{-1}, the Ti—O and Zr—O stretches (8) were observed.

The presence of significant amounts of CO_2 in the pyrolysis of PZT gels was confirmed by FTIR, and is shown in figure 11. The gases collected during the pyrolysis of a freeze-dried A1 PZT gel on a vacuum

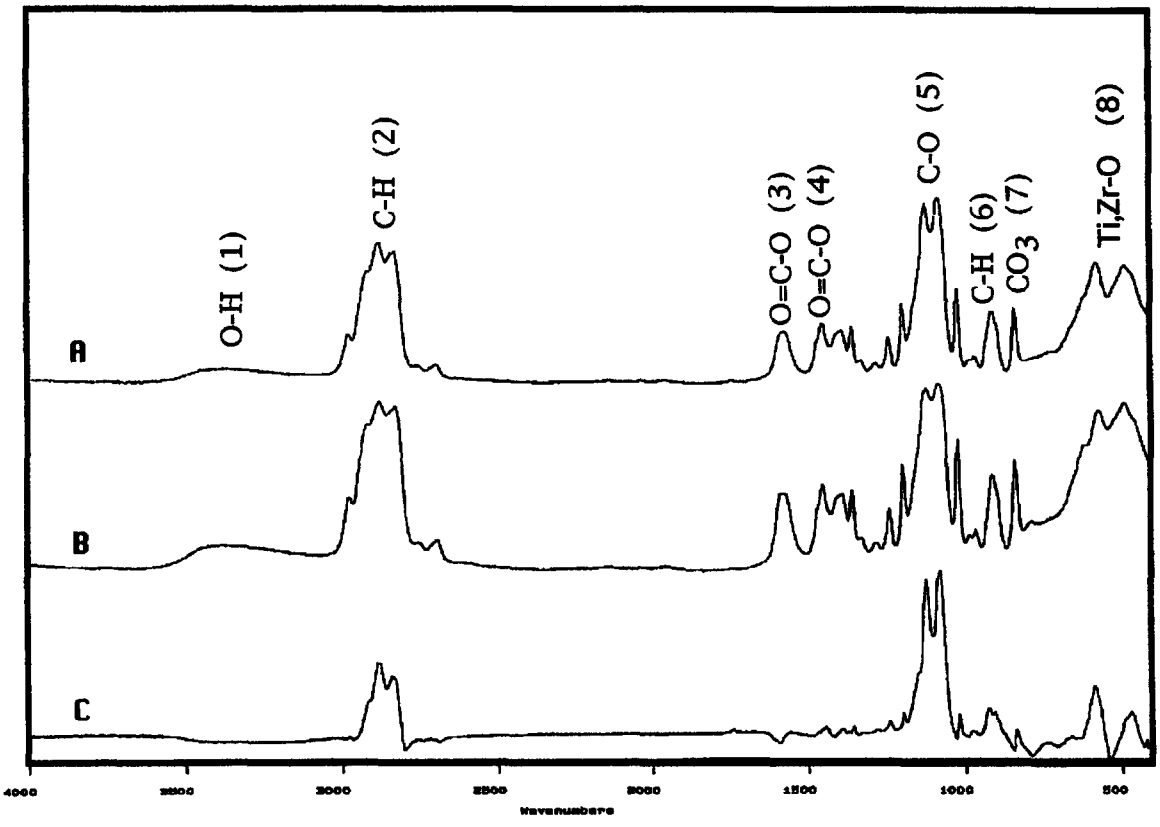

Figure 9. FTIR spectra (absorbance) of the prehydrolyzed Pb-(Zr, Ti) alkoxides prepared by (a) method I and (b) method II.

line (10^{-5} Torr) were collected in a gas cell and analyzed. There were major peaks at 2349 and 1338 cm^{-1} (figure 14) which correspond to CO_2. Other peaks confirmed the existence of acetone and methoxyethanol as volatile products. This further verifies the presence of substantial amounts of carbon dioxide detected in the DMSA studies, the main source of which is shown in Eq. 2. Thus carbonate groups, both in the room temperature (due to CO_2 absorption) and as a result of the thermal decomposition of acetate ligands (via Eq. 2), have been positively identified in the gel structure.

One related DMSA observation which explains the origin of carbonate groups in the freeze-dried A1 and B1 PZT gel merits a few comments. Dried gels which had been exposed to air for a significant time had a higher initial CO_2 evolution compared to the freshly prepared dried gels. This indicated that carbonate groups can form via carbon dioxide uptake from the air. Since lead carbonate does not decompose until 650°C, it is recommended that sols and dessicated gels not be exposed to the atmosphere for prolonged lengths of time.

3.3. Pyrolysis of PT and PZT Gels in Oxygen

TGA/DTA was also carried out for A1 and B1 PZT and PT gels in an oxygen atmosphere (figure 12a and b) in order to simulate typical thin film processing conditions. Table 2 summarizes these results. Initial weight loss of the gels (up to ~300°C) was also much higher, and the rate much faster, in B1 compared to A1 gels. This may be explained qualitatively on the basis of the differences between acid and base catalyzed gels. Since acid-catalyzed gels can shrink and densify readily at low temperatures, unburned organic can be trapped within the dense structures. In contrast, the highly cross-linked base-catalyzed gels facilitate the removal of organic through its open structures. Therefore, acid-catalyzed gels are expected to have higher residual organics.

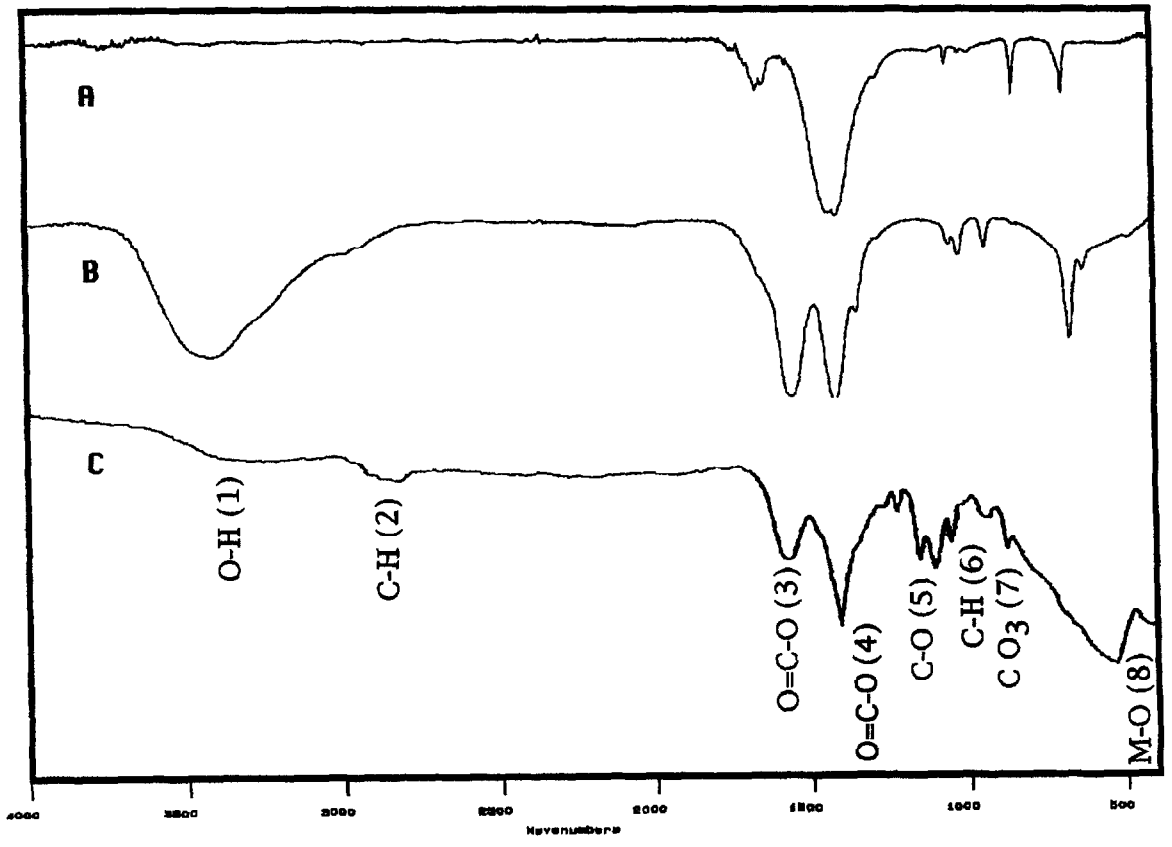

Figure 10. FTIR spectra (transmittance) of (a) lead carbonate (b) lead acetate trihydrate (c) freeze-dried A1 PZT gels.

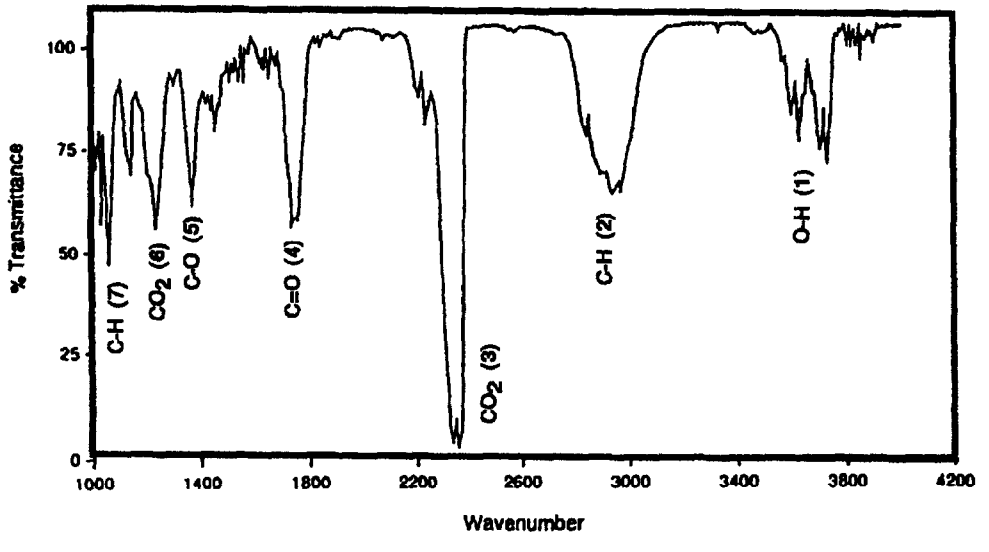

Figure 11. FTIR spectrum (transmittance) of gases evolved in the pyrolysis of A1 freeze-dried PZT gel.

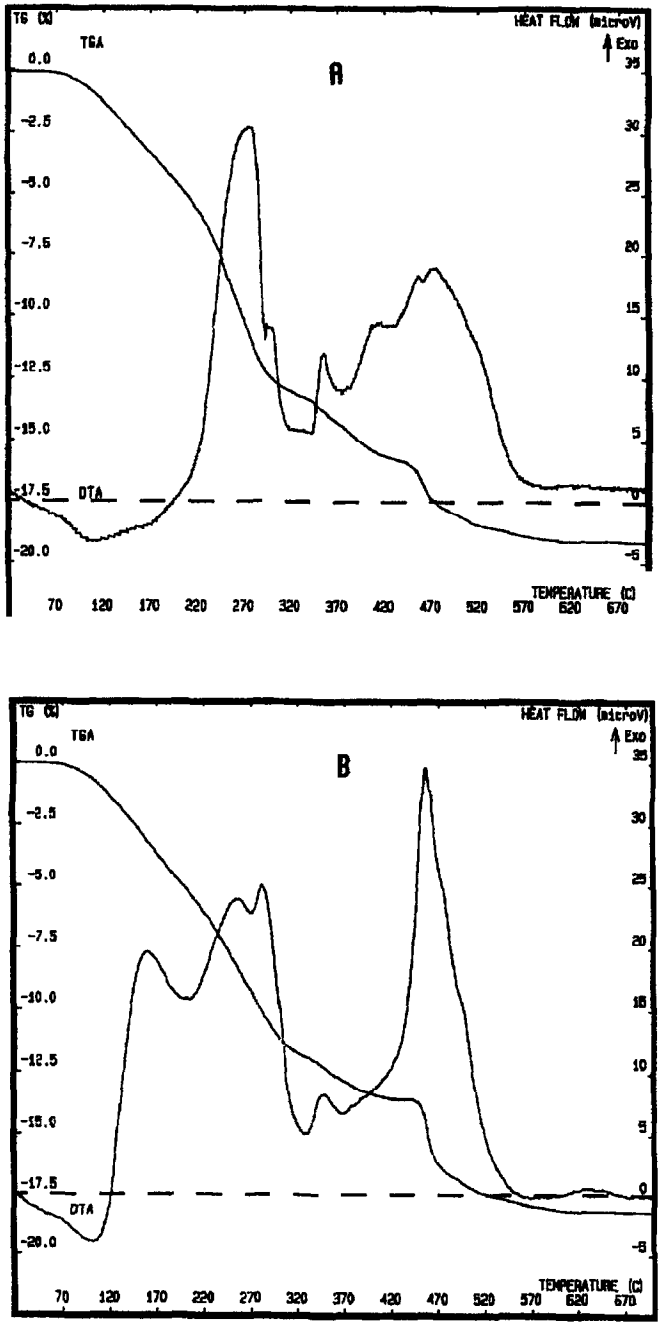

Figure 12. TGA/DTA curves for (a) A1 and (b) B1 PZT gels in oxygen.

Similar to the silica system, acid-catalyzed gels always had higher weight loss than base-catalyzed gels. For the silica system, higher weight loss in acidic gels compared to basic gels is a result of a lower degree of phase separation and a higher number of terminal alkoxy groups in acid-catalyzed gels [19]. However, while there is a large difference in weight loss of the silica system, only a small difference in weight loss is observed in A1 vs. B1 PZT and PT. This is a direct result of the low concentration of catalyst in this study.

In A1 PZT, there was a broad endotherm from 20–200°C again due to 1) the vaporization of adsorbed water and ROH at lower temperatures and 2) the volatilization of trapped solvent at higher temperatures. This was followed by four large exothermic peaks which were observed at 260, 345, 420, and 475°C due to the combustion of organics. A small peak was observed at 615°C, which was the crystallization exotherm. In B1, there was a broad endotherm at 20–120°C, which was due to the volatilization of adsorbed water and ROH. This was followed by five large exotherms at 155, 250, 280, 345, and 475°C. The crystallization exotherm was observed at 635°C for B1 compared to 615°for A1, which was to be expected.

The DTA of A1 and B1 PT are given in figures 13(a, b), respectively. The details of the exothermic and endothermic events are given in Table 2. Note that a higher number of exotherms were observed in base-catalyzed gels compared to acid-catalyzed gels. No exotherms due to crystallization were observed. It should be stressed that by 200°C, A1 is still vaporizing ROH (due to trapped solvent), while B1 has already gone through one exothermic decomposition process (due to condensation polymerization).

The multiple exothermic peaks in these DTA curves at temperatures 200°C are due to the oxidation of various ligands (e.g., acetate, alkoxy) which reside in different chemical environments. Both acid and base-catalyzed PT gels completed their weight loss by ~500°C, whereas acid and base-catalyzed PZT gels completed their weight loss by ~600°C. The higher decomposition temperatures of PZT gels versus PT gels is due to the higher decomposition temperature of the zirconium component. The decomposition patterns for PZT and PT gels were similar towards the completion of oxidation (negligible weight loss and heat flow).

The weight losses of A1 and B1 PZT and PT in an oxygen ambient was lower than in helium. A probable explanation is the loss of oxygen due to the reduction of PZT by carbonaceous residues in helium. This was proven by two specific TGA experiments using stoichiometric A4 gels. The first experiment was comprised of two sequential TGA runs; one run in He (figure 14a) was followed by one in O_2 using the same sample (figure 14b). The second experiment was carried out solely in oxygen (figure 15). In the first experiment, a weight loss of 15.2% and a 3.3% weight gain were observed from figures 14(a, b), respectively. The result of these two runs was a net 11.9% weight loss. Corresponding XRD data indicated that after the first run in He, the phases identified were perovskite, pyrochlore, and metallic lead. After the second run in oxygen, phase pure perovskite resulted. Figure 15 illustrates a 12.6% weight loss in the second experiment, which resulted in phase pure perovskite. The result of this second experiment was in good agreement with the net 11.9% found in the first experiment. Gels prepared by method II show a lower weight loss both in helium and oxygen, with the weight loss complete by 500°C. This is the direct result of a lower amount of alkoxy groups in the prehydrolyzed precursor (see Section 3.2) compared to the method I product.

Powder X-ray diffraction of the powders, obtained after calcination inside the TGA/DTA analyzer, have been carried out to identify the phase present. In the case of A1 PZT gels calcined in an oxygen atmosphere, the XRD of the powders indicated the presence of tetragonal and orthorhombic PbO, besides the PZT phase (figure 16a). However, only orthorhombic PbO, besides the perovskite phase, is observed in the case of B1 gels (figure 16b).

3.4. *Effects of Acid/Base Catalysis and Method I/II Solution Synthesis on Thin Film Microstructures*

The effect of the catalyst upon the thin film microstructures of A1 and B1 PZT thin films are shown in figures 17(a, b), respectively. As discussed before, the acid-catalyzed gels attain a very low energy amorphous structure, requiring only minimal energy to undergo transformation to the crystalline state [16]. This favors a higher nucleation density which eventually leads to smaller grain size. Indeed, the grain size for A1 (0.2–0.3 μm) was smaller than that of B1 (0.5–0.7 μm), as expected. In contrast, a previous study [20] was unable to explain why sol-gel derived PZT powders obtained from acid-catalyzed gels with low water content had a larger grain size and were less porous than

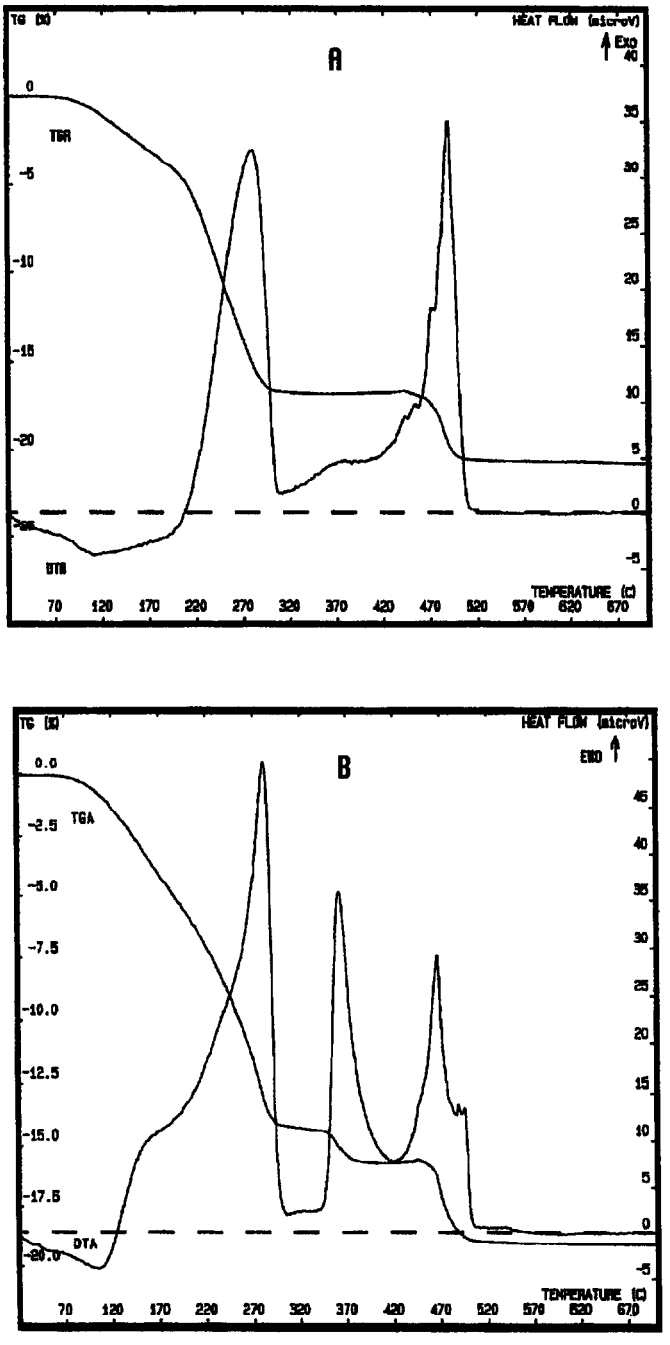

Figure 13. TGA/DTA results for (a) A1 and (b) B1 PT gels in oxygen.

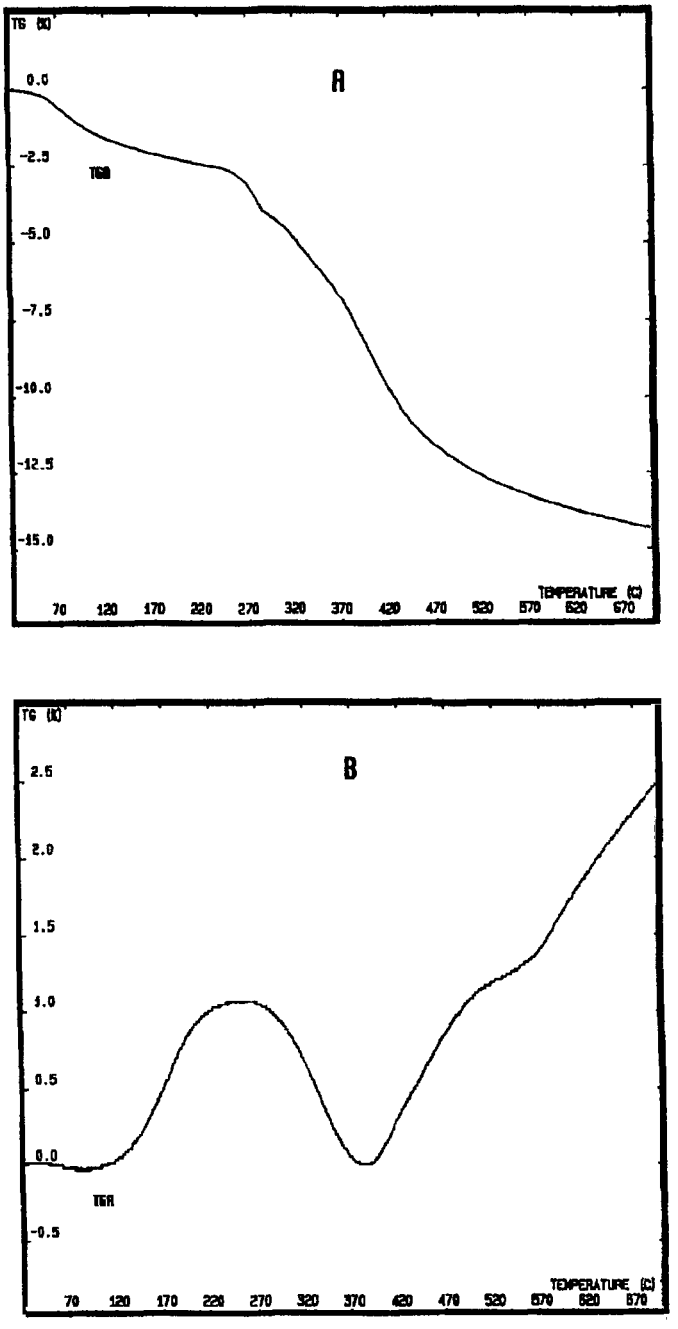

Figure 14. TGA curve of A4 PZT gel (a) pyrolyzed in He (b) followed by heating in O_2.

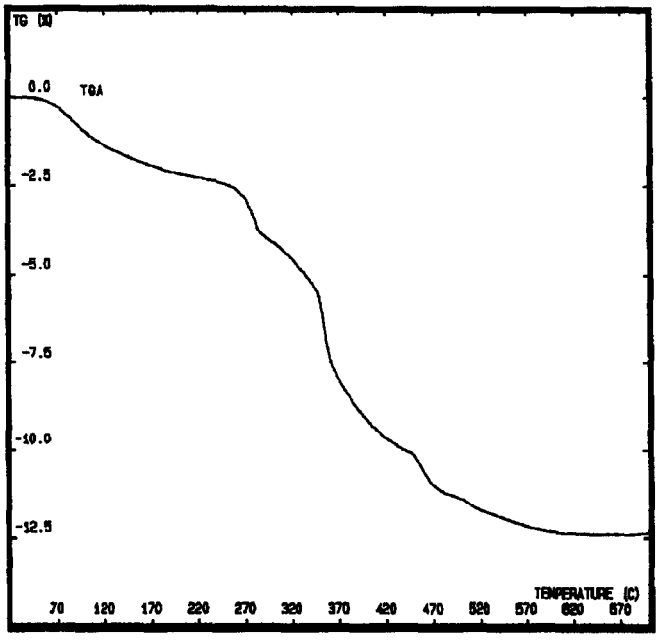

Figure 15. TGA curve of A4 PZT gel pyrolyzed solely in O_2.

powders derived from base-catalyzed gels with high water content. Additionally, their direct comparison between acid and base-derived powders is questionable since different amounts of hydrolysis water were used to form the gels.

To achieve a dense crystalline thin film, it is important to obtain a dense, amorphous film prior to crystallization [21]. Since acid-catalyzed gels are nanocrystalline at low temperatures (300–400°C) [16], densification prior to crystallization is difficult. A dense, closed-packed lamellar structure of acid-catalyzed gels trap higher residual organics. Therefore, a clean pyrolysis is difficult. This leads to cracking tendencies in thin films and porosity within the rigid crystalline matrix. The removal of these pores requires extreme thermal treatments. Since base-catalyzed gels undergo a sluggish reconstructive transformation to the crystalline state [15, 16], densification to the amorphous film can occur before crystallization [22].

Stock solutions obtained by methods I and II were used to fabricate films. The films were crystallized and densified using rapid thermal annealing, RTA, which had a heating rate of 250°C/sec, instead of a rod of 15°C/min with conventional firing. SEM microstructures of PZT thin films obtained from the prehydrolyzed solutions synthesized by methods I (B1) and II (B2) are illustrated in figures 18(a, b), respectively. Note that a substantial reduction in porosity is achieved in B1 films as a result of using RTA. Also, a decrease in carbon content was found by Electron Energy Loss Spectroscopy (EELS) [23] since a rapid heating rate allows free organics to vaporize instantaneously due to the open structure created during rapid thermal expansion. Volatiles from thermolytic or combustion processes are also easily removed from this open structure. Note that residual carbon species from the decomposition of residual organic groups are always present in the final product. One study has confirmed these carbon containing areas which surround the pores [23]. The use of synthetic method II reduces the amount of alkoxy groups and thus leads to a cleaner burnout and a cleaner microstructure. Also, note that the grain size is smaller in the B1 PZT films prepared by RTA (figure 18a) compared to the B1 films prepared by conventional firing (figure 17b). This is due to the fact that for a faster heating rate, crystallization occurs at a higher temperature, therefore the nucleation rate is higher, leading to a smaller grain size.

In terms of processing conditions for PZT powders and thin films, base catalyzed high water content sols prepared by method II coupled with rapid thermal annealing are preferred. This is based on the fact that shrinkage and cracking are minimized due to the lower weight loss associated with a lower organic content. Finally, the more open base-derived structure as opposed to the closed, dense acid-derived structure facilitates

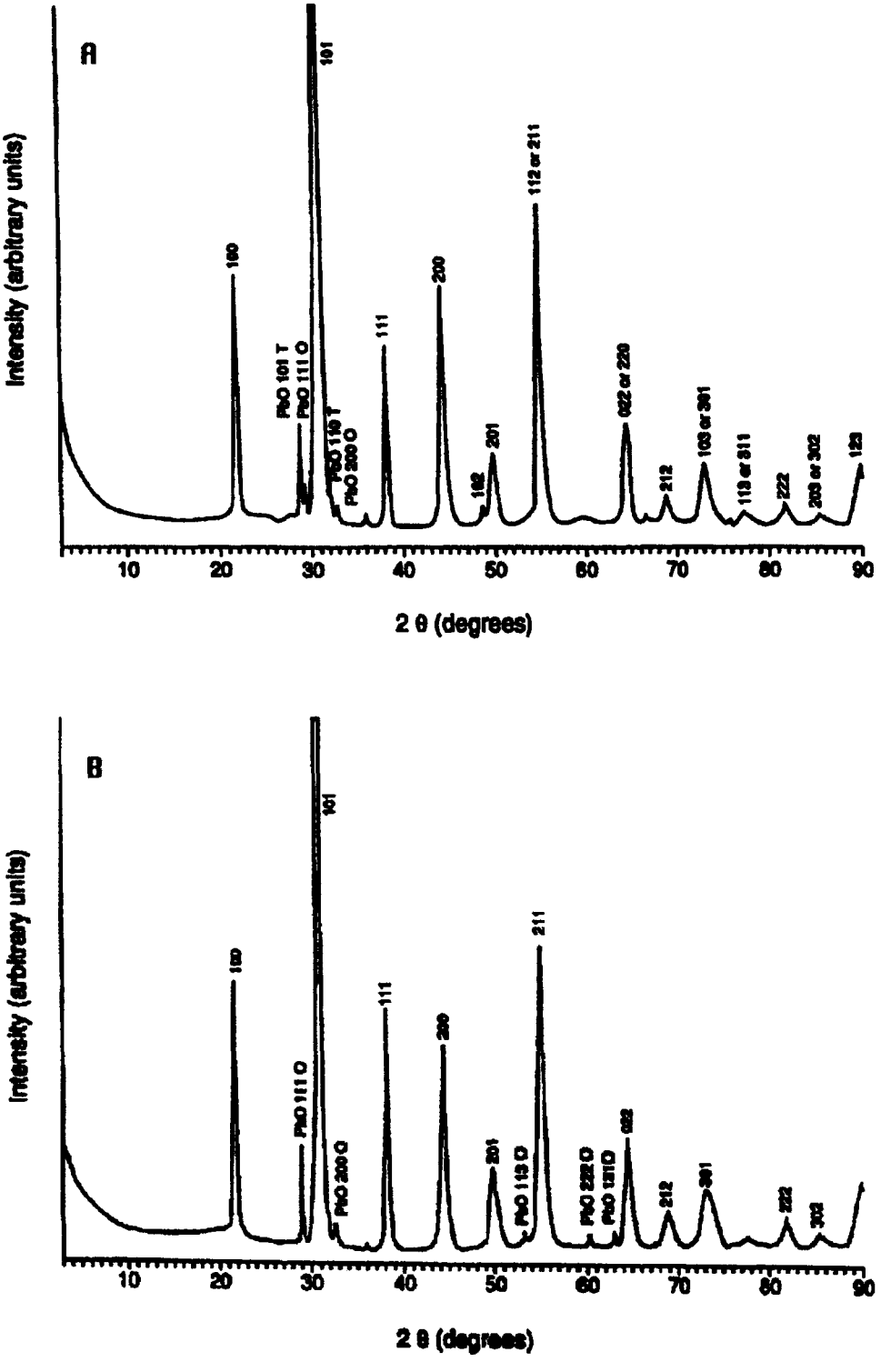

Figure 16. XRD of pyrolyzed (a) A1 (b) B1 PZT gels.

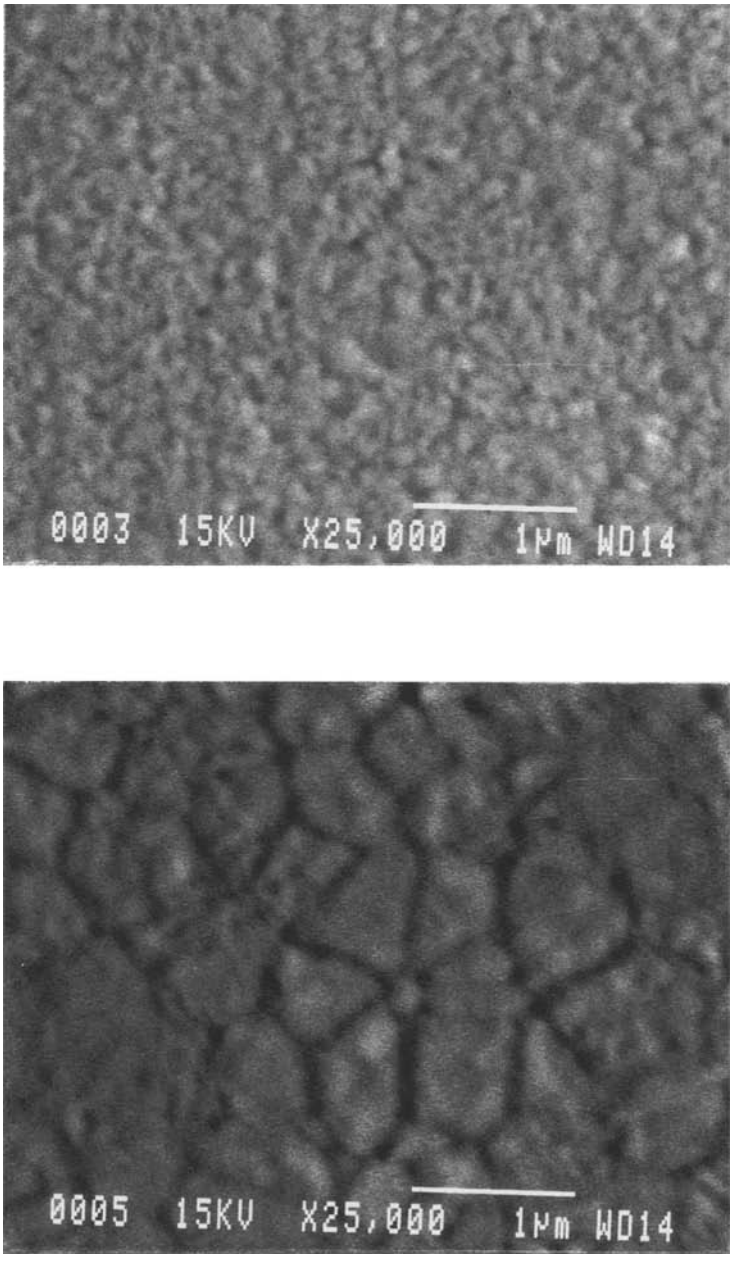

Figure 17. SEM microstructures of (a) A1 PZT thin film and (b) B1 PZT thin film.

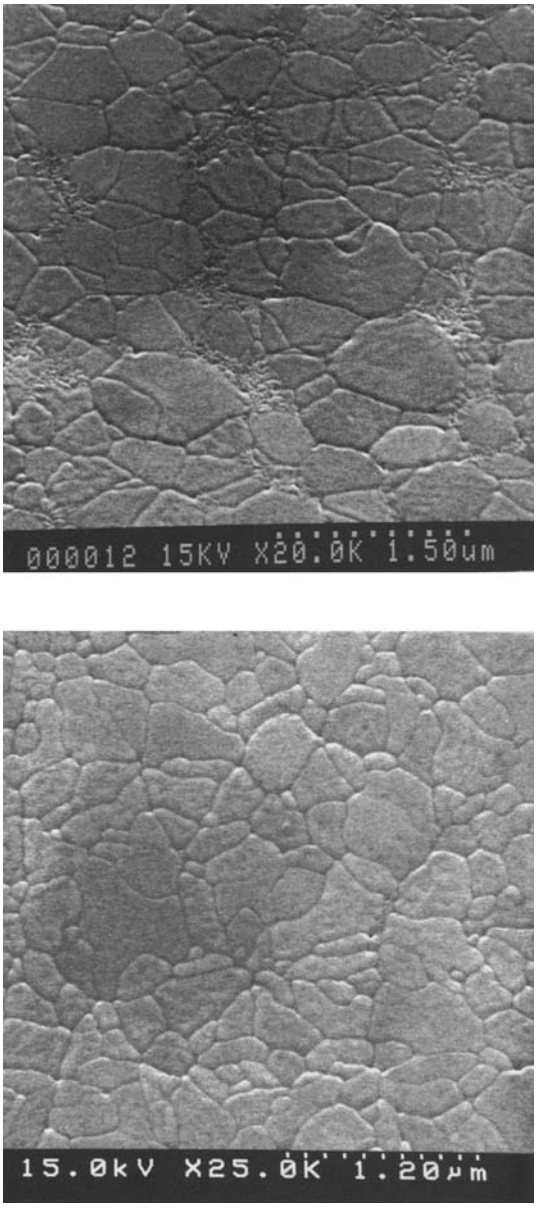

Figure 18. SEM microstructures of a PZT thin film prepared from solutions made by (a) method I and (b) method II.

the removal of residual organics during rapid thermal annealing.

4. Conclusions

In this study, it was discovered that the differences in the synthetic methods (I and II) of the prehydrolyzed precursor and the structural differences between acid vs. base-catalyzed gels, affect the structural evolution of sol-gel derived PZT gels and thin films. It was clearly demonstrated that the residual acetate, alkoxy, and carbonate groups as well as hydrolysis conditions influenced the pyrolytic behavior of the gels and thin-film microstructure. Based on the understanding of structure evolution in the silica system, the various events in the DTA/TGA studies of acid-catalyzed PZT gels were attributable to specific mechanisms. Some salient features of this study along with the key processing issues are summarized below.

Infrared spectroscopy demonstrated that residual acetate groups remained attached to the structure in freeze-dried and oven-dried gels. Reduced amounts of unhydrolyzed alkoxy groups were present in the prehydrolyzed PZT precursor when the reaction time between lead acetate and 2-methoxyethanol was increased to 24 hrs (Method II). This lead to a lower weight loss associated with gels derived from method II solutions.

The microstructures of PZT thin films obtained from acid-catalyzed sols showed smaller grain size than those prepared from base-catalyzed gels. This result was explained by the high initial nucleation density achievable in acid-catalyzed gels. Here lies an independent avenue of tailoring the grain size of thin films.

From a processing point of view, base-catalyzed high water sols are preferred for two reasons: 1) Since the crystallization is sluggish in highly cross-linked gels, complete gel (amorphous) densification may be achieved prior to crystallization. This is necessary to obtain dense, crystalline films; 2) Due to its open structure, evolution of trapped organics is facilitated during drying and, therefore, the observed weight loss during the pyrolysis is small. Consequently, the cracking tendencies of the thin films are reduced. It should be noted that base-catalyzed gels, pyrolyzed in helium, showed a higher amount of elemental lead as expected. The implications of this result of this result will be the subject of a future publication.

In addition to the decomposition of acetate groups via the carbonate route, another source of carbonate groups appears to be absorbed carbon dioxide from the air. Since these carbonate groups do not decompose until high temperature, it is recommended that sols be stored in air-tight containers.

Finally, the removal of residual organics followed by the densification of the amorphous gel-matrix in thin films, prior to crystallization, was possible by using

a rapid rate of heating (250°C/s) in a RTA furnace. A decrease in carbon content was found since a rapid heating rate allows free organics to vaporize instantaneously due to the open structure created during rapid thermal expansion. Also, volatiles from thermolytic or combustion processes are easily removed from this open structure.

Acknowledgments

This work was funded by MTO at ARPA. The X-ray data was obtained on an instrument purchased under National Science Foundation grant DMR-8406823. Thermal analysis was performed in the Materials Preparation Facility in the Center for Solid State Science. The authors would like to thank T. Karcher, S. Nemani, J. Finder and D. Wright for some experimental assistance and Drs. M. McKelvy, J. Lehman, and A.M. Yates for their helpful discussions.

References

1. P.R. Coffman and S.K. Dey, J. Sol-Gel Sci. Tech. **1**(3), 251 (1994).
2. J.B. Blum and S.R. Gurkovich, J. Mater. Sci. **20**, 4479 (1985).
3. K.D. Budd, S.K. Dey, and D.A. Payne, Brit. Ceram. Soc. Proc. **36**, 107 (1985).
4. Y. Hayahi and J.B. Blum, J. Mater. Sci. **22**, 2655 (1987).
5. S. Li, R.A. Condrate, Sr., and R.M. Spriggs, Spectrosc. Let. **21**(9/10), 969 (1988).
6. B.A. Tuttle, R.W. Schwartz, D.H. Doughty, and J.A. Voigt, Mater. Res. Symp. Proc. **200**, 159 (1990).
7. C.-C. Hsueh and M.L. Mecartney, J. Mater. Res. **6**(10), 2208 (1991).
8. C.D.E. Lakeman, J.-F. Campion, and D.A. Payne in *Ferroelectric Films, Ceramic Transactions, Volume 25*, edited by A.S. Bhalla and K.M. Nair (American Ceramic Society, Westerville, OH, 1992), p. 413.
9. C.D.E. Lakeman and D.A. Payne, J. Am. Ceram. Soc. **75**(11) 3091 (1992).
10. A.P. Wilkinson, J.S. Speck, and A.K. Cheetham, Chem. Mater. **6**, 750 (1994).
11. D.F. Shriver and M.A. Drezdzon, *The Manipulation of Air Sensitive Compounds* (Wiley-Interscience, New York, 1986).
12. S.K. Dey and R. Zuleeg, Ferroelectrics **108**, 37 (1990).
13. EPA/NIH Mass Spectral Data Base.
14. C.K. Barlingay and S.K. Dey, Ceramic Transactions, Ferroelectric Films **52**, 265–270 (1992).
15. S.K. Dey, K.D. Budd, and D.A. Payne, J. Am. Ceram. Soc. **70**(10), C-295–C-296 (1987).
16. Z.C. Kang, S.K. Dey, and L. Eyring, Mat. Res. Soc. Proc. **180**, 291 (1990).
17. C.J. Brinker and G.W. Scherer, *Sol-Gel Science* (Academic Press, New York, 1990), Ch. 9.
18. S. Doeuff, M. Henry, C. Sanchez, and J. Livage, J. NonCryst. Solids **89**, 206 (1987).
19. K.D. Keefer, Mat. Res. Soc. Proc. **32**, 15 (1984).
20. R.W. Schwartz, C.D.E. Lakeman, and D.A. Payne, Mat. Res. Symp. Proc. **180**, 335 (1990).
21. C.K. Barlingay and S.K. Dey, Proc. of the Symp. on Rapid Thermal and Integrated Processing, MRS Spring Meeting, Anaheim CA, Mat. Res. Soc. **224**, 311–316 (1991).
22. K.D. Budd, S.K. Dey, and D.A. Payne, Mat. Res. Soc. Symp. Proc. **73**, 711 (1986).
23. A. Modak and S.K. Dey, Integrated Ferroelectrics (in press).